Application of Artificial Neural Network to Computer-Aided Diagnosis of Coronary Artery Disease in Myocardial SPECT Bull's-eye Images

Hiroshi Fujita, Tetsuro Katafuchi, Toshiisa Uehara, and Tsunehiko Nishimura*

Department of Electronics and Computer Engineering, Gifu University, Yanagido, Gifu, Japan and Department of Radiology, National Cardiovascular Center, Suita, Osaka, Japan

We have developed a computerized system that can aid in the radiologist's diagnosis in the detection and classification of coronary artery diseases. The technique employs a neural network to analyze ^{201}Tl myocardial SPECT bull's-eye images. This multi-layer feed-forward neural network with a backpropagation algorithm has 256 input units (pattern: compressed 16 × 16-matrix images), 5–140 units in a single hidden layer, and eight output units (diagnosis: one normal and seven different types of abnormalities). The neural network was taught using pairs of training (learning) input data (bull's-eye "EXTENT" image) and desired output data ("correct" diagnosis). The effects of the numbers of hidden units and learning iterations in the network on the recognition performance were examined. In our initial stage, the results show that the recognition performance of the neural network is better than that of the radiology resident but worse than that of the experienced radiologist. Our study also demonstrates that the result produced in the neural network depends on the variety of the training examples used. The preliminary study suggests that the neural network approach is useful for the computer-aided diagnosis of coronary artery diseases in myocardial SPECT bull's-eye images.

J Nucl Med 1992; 33:272–276

Visual interpretation of nuclear images, even by experienced observers, is subject to substantial variability (1). Thallium-201 myocardial SPECT imaging has been reported to offer major improvements over planar imaging and to be sensitive and specific examination for the diagnosis of coronary artery disease. However, to overcome the difficulties of the interpretation of the myocardial SPECT images, a polar map display, called a bull's-eye image, has been developed to characterize the three-dimensional images of the left ventricle in two dimensions.

Even with the bull's-eye technique, many problems have been indicated as follows: (a) lesions occupying the boundary zone are problematic in identifying the responsible coronary artery, (b) continuous lesions by multivessel disease are sometimes misdiagnosed as single-vessel disease, (c) lesions in the basal area are visually larger than those in the apical area when displayed, and (d) lesions are sometimes misread as artifacts. The development of a computer-aided diagnostic system (*2–7*) or expert system, therefore, is considered to be helpful in the field of nuclear medicine. For example, consultation expert systems have been developed with use of the artificial intelligence (AI) technique (*8–10*).

The purpose of this paper is to develop a computerized system that can aid in the radiologist's diagnosis in the detection and classification (pattern recognition) of coronary artery diseases in ^{201}Tl SPECT bull's-eye images by use of an artificial neural network. Although neural network applications are starting to appear in the radiology literature (*11–15*), we cannot find any successful examples that treat image pattern as an input to the network. One possible reason is the large volume of data in medical radiographic images. However, nuclear images with a 64 × 64 matrix provide a basis for testing the concept. One of the advantages of the neural network approach is its powerful ability to analyze the complicated decision-making or pattern-recognizing process in diagnosis without any need to write a special computer program. As a pilot study, we investigated the applicability of the neural network technique in the computer-aided diagnosis of coronary artery diseases in ^{201}Tl SPECT images based on measurements by a bull's-eye image data base. The recognition performance of the neural network was compared with that of residents and radiologists. The effects of image data combinations on learning and testing, the number of hidden units, and the number of learning iterations on network performance were examined.

MATERIALS AND METHODS

Thallium Myocardial SPECT Imaging

The bull's-eye technique synthesizes three-dimensional information from ^{201}Tl myocardial SPECT images into a two-dimen-

Received May 29, 1991; revision accepted Sept. 9, 1991.
For reprints contact: Hiroshi Fujita, PhD, Department of Electronics and Computer Engineering, Gifu University, Yanagido, Gifu 501-11, Japan.

sional display so that patient data can be compared quantitatively against normal data. Coronary artery territories in the bull's-eye display are illustrated in Figure 1 (*16*), where the regions of three main coronary arteries, left anterior descending coronary artery (LAD), right coronary artery (RCA), and left circumflex coronary artery (LCX), are segmented. Coronary artery diseases can therefore be classified into seven different types due to the existence of single-, double-, and triple-vessel diseases.

Thirty-six planar images of 64 × 64 matrix and 64 gray levels were obtained (30 sec/view) with a gamma camera (Shimadzu LFOV dual-head) and these data were transferred to a data processing system (Shimadzu SCINTIPAC-2400) at the Department of Radiology, National Cardiovascular Center. This system produces three different types of bull's-eye images at the same time, i.e., "PIXEL CT", "EXTENT", and "SEVERITY" images, which respectively represent the original bull's-eye image, the image simply showing only the extent area of disease relative to the averaged normal case, and the image showing the severity within the extent area. In this pilot study, we used only the bull's-eye EXTENT images for the analysis using the neural network.

Artificial Neural Networks

An artificial neural network is a computational model based upon the human brain. It has been found that the neural network is a powerful tool for pattern recognition, signal processing, image or speech data compression, learning expert systems, and so on.

We employed a personal neuro-computer system (Neuro-07, NEC), which consists of a 16-bit personal computer (PC-9801 VX21 with 10-MHz CPU (80286), NEC) a neuro-engine board (PC-98XL-02, NEC), and a neuro-software package ("Michi-Zane", NEC). This board, called "ImPP board" (*17*), has four original data flow pipeline processors (μ PD7281), all of which can carry out processing in parallel. The neural network software written in C language is based upon a feed-forward layered model with an input layer, one to three middle or hidden layer(s), and an output layer (Fig. 2), on which a so-called backpropagation learning model is implemented (*18*).

Image patterns or digitized images of matrix size of n × n (n = positive integers) are given onto the n^2 neurons or units in the input layer. Each unit in the network corresponds to a pixel in the image. "Synapses" connect neurons in the input layer and in the hidden layer, and also ones in the hidden layer and in the output layer. Each of these synapses is associated with a weight value. After calculations through feed-forward propagation using values on these synapses and on neurons in the lower layer, network output values are obtained in the output layer. Then a "teacher" signal is given to the network, and the backpropagation technique modifies weight values so that the summation of the squared errors in the output layer is minimized. This modification of the weight values is called a learning or training process.

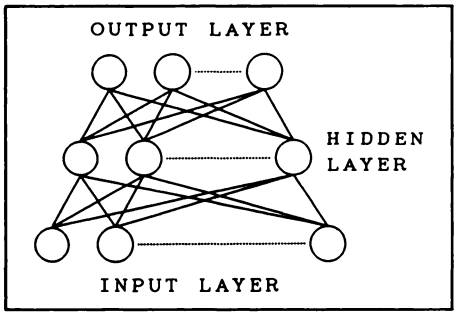

FIGURE 2. A three-layer feed-forward neural network, in which circles represent neurons or units in each layer.

The neural network becomes cleverer after repeated learning procedures, and finally begins to recognize patterns correctly, even patterns never used in the learning process (the testing or recognizing process).

Image Data Base

We collected a total of 74 bull's-eye images (Table 1) that were relatively typical cases. All of them had been examined by coronary angiography, in which a coronary artery of more than 75% stenosis was diagnosed as "disease" according to the criteria of the American Heart Association (AHA). In our pilot study, the special cases in which the diagnoses obtained by angiography and SPECT bull's-eye examinations were not identical were eliminated. These diagnosed results were employed as a gold standard or "correct diagnosis." We tried to collect the same number of patterns for each classification of coronary diseases, and ten images were prepared for each case, except the case of triple-vessel disease (only four images) due to difficulty in finding it. The combination of the data for the learning process and recognizing process was changed in the neural network analysis.

In order to compare the recognition performance of the neural network with that of radiologists, all of the EXTENT images collected were diagnosed by one radiology resident and two radiologists, whose experiences with SPECT imaging were 3 mo, 2 and 10 yr, respectively. The percent correct or recognition rate, i.e., the percentage of all of the responses that were recognized (diagnosed) to be correct, then was calculated for performance evaluation.

TABLE 1
Number of Image Data for Eight Classified Coronary Diseases Including Normal Used in Neural Network Analysis

	Learning	Recognizing	Total
Normal	8	2	10
LCX	8	2	10
RCA	8	2	10
LAD	8	2	10
AX (= LAD + LCX)	8	2	10
XR (= LCX + RCA)	8	2	10
AR (= LAD + RCA)	8	2	10
AXR (= LAD + LCX + RCA)	2	2	4
Total	58	16	74

LCX = left circumflex coronary artery, RCA = right coronary artery, and LAD = left anterior descending coronary artery.

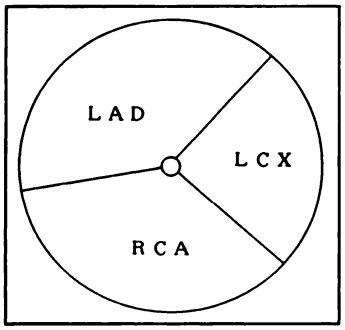

FIGURE 1. Coronary artery territories in the bull's-eye display from ref. 16.

Methods

A block diagram illustrating the overall procedure of our approach is shown in Figure 3. The bull's-eye images on the instant picture were sent to the Laboratory of the Gifu University (off-line method for our initial investigations). These pictures were initially read using a color image scanner (Epson GT-1000) to produce images with a 96 × 96 matrix and 256 gray levels.

Due to the memory capacity limitation of the neuro-engine board, preprocessing of image data is required. This is also important in order to save computation time. Therefore, most of the digital images studied in the present paper were compressed to produce images of 16 × 16 matrices by averaging the neighboring pixel values and also to produce binary (black and white) gray level images. A digitized image with a 96 × 96 matrix and binary gray level is shown in Figure 4A, which is a case of LCX disease. Figure 4B is a 16 × 16 matrix binary level image obtained from the image shown in Figure 4A. These compressed images were employed as an input to the neural network.

The number of neurons in the output layer was fixed to eight units corresponding to eight different types of diagnoses, including normal. The neural network was trained using pairs of training input images (compressed EXTENT images) and the desired output data ("correct diagnosis" based on the gold standard).

The number of neurons or units in the hidden layer was varied. The effects of the numbers of hidden units and learning iterations in the network on the recognition performance were examined.

RESULTS

As explained in the previous section, we varied combinations of image data for the learning and recognizing processes in the neural network and made three different combinations, cases A, B, and C, in which all images were chosen at random from a data base of 74 images. In our study, the network involves one hidden layer with 100 hidden units and 200 learning iterations. After the learning iteration, all 58 images used for learning were recognized correctly during the recognition process. The recognition results by the neural network (NN), one resident (I), and two radiologists (II and III) are shown in Table 2, in which the number of correctly recognized images out of 16 and the recognition rate are listed. Table 2 also demonstrates that recognition rate depends on the image combinations. The range of change in recognition rate among the three cases are up to 19%, 25%, and 13% for NN, resident, and radiologists, respectively. This can be explained from two different viewpoints. One is that the image data used for the learning iteration may be insufficient for recognizing testing image data. The other is that the variety of image data and its categorization in the learning process and the degree of difficulty in diagnosing in the recognition process may cause variances in the recognition rate. These effects may be decreased by increasing the image data for learning as well as for recognition. By comparing the averaged results, the performance of the neural network is better than that of the resident, and comparable to that of the 2-yr experienced radiologist, but worse than that of the 10-yr experienced radiologist.

Table 3 illustrates an example of the neural network output in Case B in Table 2. The confidence level is determined from the weight values in the output layer. The ideal case is such that the first candidate has a high

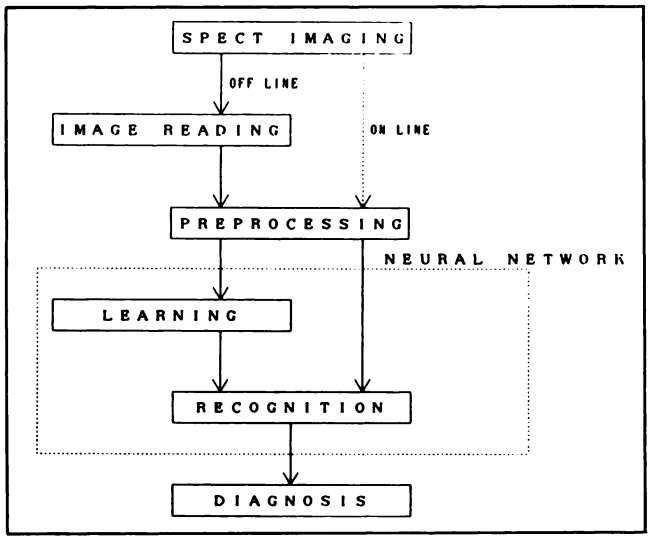

FIGURE 3. Overall procedure for the analysis of bull's-eye images by the neural network.

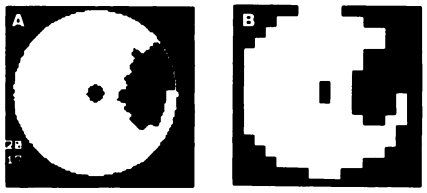

FIGURE 4. (A) A digitized image of a 96 × 96-matrix and binary level in a case of LCX disease. (B) A compressed image of a 16 × 16-matrix and binary level determined from the image shown in (A).

TABLE 2
Number of Correctly Recognized Images (Percentage of Correct Recognition) for Three Different Combinations of Image Data

	Case A	Case B	Case C	Average
NN	11 (69%)	12 (75%)	14 (88%)	12.3 (77%)
I	9 (56%)	13 (81%)	11 (69%)	11.0 (69%)
II	12 (75%)	12 (75%)	14 (88%)	12.7 (79%)
III	12 (75%)	14 (88%)	14 (88%)	13.3 (83%)

NN = neural network; I = three-month RI experienced resident; II = 2-yr RI experienced radiologist; and III = 10-yr RI experienced radiologist.

TABLE 3
An Example of Neural Network Recognition (Case B in Table 2)

Category name of input data	Candidate (confidence level) in output			
	First		Second	
Normal	NOR	(0.886)	LCX	(0.074)
Normal	NOR	(0.954)	LCX	(0.027)
LCX	LCX	(0.984) [I, II]	AX	(0.562)
LCX	LCX	(0.991) [II]	AX	(0.044)
RCA	RCA	(0.978)	AR	(0.010)
RCA	RCA	(0.995)	NOR	(0.041)
LAD	LAD	(0.977)	AXR	(0.034)
LAD	LAD	(0.997)	AX	(0.030)
XR	AR *	(0.861)	XR	(0.476)
XR	XR	(0.994) [III]	LCX	(0.003)
AR	LAD *	(0.657) [II]	AX	(0.169)
AR	AR	(0.126) [I]	AXR	(0.050)
AX	AX	(0.922)	LAD	(0.418)
AX	AX	(0.994)	LAD	(0.346)
AXR	AR *	(0.136) [I]	XR	(0.094)
AXR	AX *	(0.991) [II, III]	LCX	(0.480)

* Incorrect recognition by first candidate.
Number in brackets is name of the resident [I] or radiologist [II, III] who incorrectly diagnosed the image.
See Tables 1 and 2 for abbreviations.

confidence level but the second candidate has a low confidence level, as are most of the cases in Table 3. On the other hand, special attention should be paid to the cases such as the first candidate with a low confidence level or the second candidate with a high confidence level, which are specifically applied to the four incorrectly recognized images (shown by *) in the table. For these cases, the computer can therefore give a "warning" to the physician. Both of the images for triple-vessel disease (AXR) were incorrectly diagnosed by both the neural network and the physicians. Moreover, most cases were recognized as the double-vessel disease, a generally acceptable diagnosis. In some cases, the image incorrectly diagnosed by the physician was correctly recognized by the network, and vice versa.

The number of hidden units was changed from 5 to 140 with the condition of one hidden layer and 200 learning iterations by using data in Case C. After the learning procedure, all of the input patterns used for the learning were recognized completely, except the cases of hidden units of 5 and 10, where two or one of the input patterns were/was incorrectly recognized. When the number of hidden units was 5 or 120, the number of incorrect recognitions was four. When the hidden units were 10, 20, 40, 60, 80, 100, or 140, the number of incorrect recognitions was two; in all of the cases except in 20, triple-vessel disease was recognized as double-vessel disease. From the viewpoint of the processing time for learning, a larger number of hidden units required longer computation time. For example, when the number of hidden units is 20 and 100, the pure computation time for learning was approximately 8 and 23 min, respectively. However, the time for learning is not so important, because the user at the hospital may simply utilize the results obtained from the learning process. On the other hand, from the viewpoint of the confidence level, it is optimum that the first and second candidate have high and low confidence levels, respectively. Finally, we selected the number 100 for the hidden units in this study because this condition is close to the "optimum." In addition, under these conditions, the recognition of a testing image in the recognition process, including the image data compression procedure, was performed in "real time."

The effects of the learning iterations on percent correct and errors are investigated by use of the learning data in Case C in Table 2 under the condition of one hidden layer with 100 hidden units. Figure 5 shows a plot indicating the relationship between the number of incorrectly recognized patterns (NIRP) or the summation of the squared errors (SSE) and the number of learning iterations. As the learning iterations increase, the number of incorrect recognition as well as errors are decreasing, and finally reaches zero. It is obvious that 200 learning iterations are sufficient.

DISCUSSION

One of the reasons for incorrect recognition by the neural network may be related to compression ratio or matrix size, the higher the compression ratio, the lower the spatial resolution. We found that when an 8 × 8-matrix image (a higher-compressed image than a 16 × 16-matrix image) was used, the same results were obtained in some cases, but sometimes the recognition ratio decreased.

It will be worthwhile to include SEVERITY images for analysis because they can help to differentiate lesions from artifacts. Actually, for one of the experienced radiologists, we observed that recognition with both of EXTENT and SEVERITY images results in a 10% higher recognition rate relative to that only with EXTENT images. In addi-

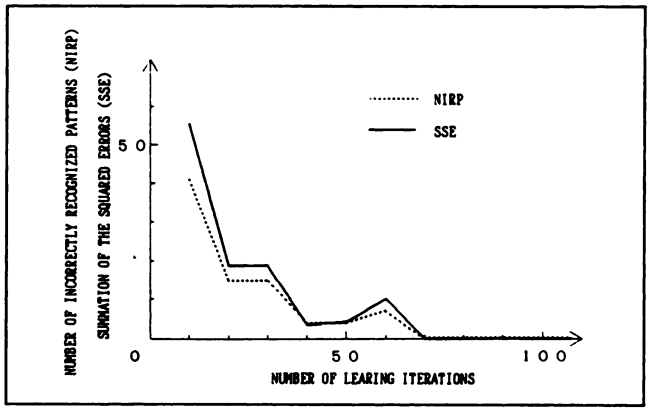

FIGURE 5. Effects of the number of training iterations on the number of incorrectly recognized patterns (NIRP) and the summation of the squared errors (SSE).

tion, because the bull's-eye maps are affected by size distributions, the use of unfolded maps (*19,20*) may be more accurate. Moreover, because image information is only one portion needed for a physician's diagnosis, other clinical information, such as sex, temperature, and cardiogram data, should be included in the overall analysis (*14, 15*).

We believe that the methodology of an artificial neural network for a computer-aided diagnostic system of coronary artery disease is effective. However, image data for the learning and testing processes should be increased. In addition, the content of the learning or training image data such as the combination of eight different kinds of images and the combination of different extent areas in each classification should be examined. Neural networks differ from AI expert systems since they do not require complicated programs for formation of rules based on capturing the knowledge of one or more experts. Neural network systems are able to form those rules by a learning procedure using pairs of training input data and desired output data. However, understanding how to effectively execute this "learning" is the key point for the neural network system; in general, one has to collect enough patterns to train the network. On the other hand, an expert system might be a better approach in the event of difficulty in preparing enough patterns to train it. Therefore, the process of learning or training can be an advantage of the neural network approach as well as a disadvantage. Moreover, hybrid systems, called "expert networks," which include both neural networks and expert systems, may be useful for further complicated applications, as discussed by others (*21*).

In conclusion, the neural network approach in our preliminary study appears to show considerable promise for computer-aided diagnosis of bull's-eye images, although continuing work is needed for improving the system up to the level of the experienced radiologist.

ACKNOWLEDGMENTS

We would like to thank Mr. H. Iida of Gifu National College of Technology (presently, Hokkaido University) and NEC Information Technologies for help with the technical assistance. We are grateful to Dr. M. Iwashita of NEC Information Technologies and Dr. D. Y. Tsai of Gifu National College of Technology for stimulating discussions. Finally, we are indebted to the radiologists and residents who participated in the decision-performance studies.

REFERENCES

1. Trobaugh GB, Wackers FJT, Sokole EB, Derouen TA, Ritchie JL, Hamilton GW. Thallium-201 myocardial imaging: an interinstitutional study of observer variability. *J Nucl Med* 1978;19:359–363.
2. Chan H-P, Doi K, Galhotra S, Vyborny CJ, MacMahon H, Jokich PM. Image feature analysis and computer-aided diagnosis in digital radiography. 1. Automated detection of microcalcifications in mammography. *Med Phys* 1987;14:538–548.
3. Fujita H, Doi K, Fencil LE. Image feature analysis and computer-aided diagnosis in digital radiography. 2. Computerized determination of vessel sizes in digital subtraction angiography. *Med Phys* 1987;14:549–556.
4. Giger ML, Doi K, MacMahon H. Image feature analysis and computer-aided diagnosis in digital radiography. 3. Automated detection of nodules in peripheral lung fields. *Med Phys* 1988;15:158–166.
5. Katsuragawa S, Doi K, MacMahon H, Nakamori N, Sasaki U, Fennessy JJ. Quantitative computer-aided analysis of lung texture in chest radiographs. *RadioGraphics* 1990;10:257–269.
6. Chan H-P, Doi K, Vyborny CJ, et al. Improvement in radiologists' detection of clustered microcalcifications on mammograms: the potential of computer-aided diagnosis. *Invest Radiol* 1990;25:1102–1110.
7. Doi K, Giger ML, MacMahon H, et al. Clinical radiology and computer-aided diagnosis: potential partners in medical diagnosis? [Abstract]. *Radiology* 1990;177(P):345.
8. Garcia EV, Ezquerra NF. Artificial intelligence comes to the clinic [Abstract]. *J Nucl Med* 1987;28:1788.
9. Goodenday LS, Cios KJ, Freasier RE: Application of machine intelligence to diagnosis of coronary stenosis [Abstract]. *J Nucl Med* 1989;30:816.
10. Horino M, Hosoba M, Wani H, et al. Development and clinical applications of an expert system for supporting diagnosis of ^{201}Tl stress myocardial SPECT. *Kakuigaku (Jpn J Nucl Med)* 1990;27:93–106 [in Japanese].
11. Boone JM, Sigillito VG, Shaber GS. Neural networks in radiology: An introduction and evaluation in a signal detection task. *Med Phys* 1990;17:234–241.
12. Boone JM. X-ray spectral reconstruction from attenuation data using neural networks. *Med Phys* 1990;17:647–654.
13. Ozkan M, Sprenkels HG, Dawant BM. Multi-spectral resonance image segmentation using neural networks. *Proc of International Joint Conference on Neural Networks 1990 (IJCNN '90)*. San Diego, CA, IEEE Catalog Number 90CH2879-5, 1990:I429–I434.
14. Asada N, Doi K, MacMahon H, et al. Neural network approach for differential diagnosis of interstitial lung diseases. *Proc of SPIE (Medical Imaging IV: Image Processing)* 1990;1233:45–50.
15. Asada N, Doi K, MacMahon H, et al. Potential usefulness of an artificial neural network for differential diagnosis of interstitial lung diseases: pilot study. *Radiology* 1990;177:857–860.
16. Garcia EV, Van Train K, Maddahi J, et al. Quantification of rotational thallium-201 myocardial tomography. *J Nucl Med* 1985;26:17–26.
17. Temma T, Iwashita M, Matsumoto K, et al. Data flow processor chip for image processing. *IEEE Trans Electron Dev* 1985;ED-32:1784–1791.
18. Rumelhart DE, Hinton GE, Williams RJ. Learning internal representations by error propagation. In: Rumelhart DE, McClelland JL, eds. *Parallel distributed processing, volume 1*. Cambridge, MA: M.I.T. Press, 1986:318–362.
19. Katafuchi T, Nishimura T, Uehara T, et al. Unfolded map of coronary artery territories by myocardial SPECT. *Kakuigaku (Jpn J Nucl Med)* 1990;27:569–577 [in Japanese].
20. Uehara T, Nishimura T, Katafuchi T, et al. Clinical evaluation of coronary territory map by using unfolded map of T1-201 myocardial SPECT. *Kakuigaku (Jpn J Nucl Med)* 1990;27:579–591 [in Japanese].
21. Eberhart RC, Dobbins RW. Systems considerations. In: Eberhart RC, Dobbins RW, eds. *Neural network PC tools: a practical guide*. San Diego: Academic Press; 1990:59–79.